U.S.NRC
United States Nuclear Regulatory Commission
Protecting People and the Environment

Technical Letter Report

TLR-RES/DE/REB-2024-14

Examining Graphite Degradation in Molten Salt Environments: A Chemical, Physical, and Material Analysis

Date:

August 2024

Prepared in response to Task 4c in User Need Request NRR-2022-009, by:

Veerappan Prithivirajan
Idaho National Laboratory

NRC Project Manager:

Joseph Bass
Reactor Engineer
Reactor Engineering Branch

Division of Engineering
Office of Nuclear Regulatory Research
U.S. Nuclear Regulatory Commission
Washington, DC 20555–0001

This report does not contain or imply legally binding requirements. Nor does this report establish or modify any regulatory guidance or positions of the U.S. Nuclear Regulatory Commission and is not binding on the Commission.

INL/RPT-23-75892

Examining Graphite Degradation in Molten Salt Environments: A Chemical, Physical, and Material Analysis

August 2024

Veerappan Prithivirajan

Idaho National Laboratory, P.O. Box 1625, Idaho Falls, ID 83415-3840

Idaho National Laboratory

INL is a U.S. Department of Energy National Laboratory operated by Batelle Energy Alliance, LLC

INL/RPT-23-75892

Examining Graphite Degradation in Molten Salt Environments: A Chemical, Physical, and Material Analysis

Veerappan Prithivirajan

Idaho National Laboratory, P.O. Box 1625, Idaho Falls, ID 83415-3840

August 2024

Idaho National Laboratory
Computational Mechanics and Materials Department
Idaho Falls, Idaho 83415

http://www.inl.gov

Prepared for the
U.S. Department of Energy
Office of Nuclear Energy
Under DOE Idaho Operations Office
Contract DE-AC07-05ID14517

EXECUTIVE SUMMARY

Molten-salt reactors (MSRs) are Generation IV nuclear reactors that use liquid salt as a coolant and/or fuel. In several MSR designs, graphite serves as a moderator and/or reflector. However, due to limited experimental data and operational experience, our understanding of graphite behavior in molten salt environments remains incomplete.

This report aims to identify the degradation mechanisms of nuclear graphite in MSRs, detail the mechanisms of each factor, and provide an initial assessment of their impact on the structural integrity of graphite components. This assessment is based on an extensive literature review and insights from subject matter experts. Furthermore, given the limited data, a modeling strategy using existing Grizzly software is proposed for a more thorough analysis where appropriate. Additionally, it presents mitigation strategies where applicable.

The report covers physical degradation mechanisms such as infiltration, erosion, and abrasion, as well as chemical degradation mechanisms including fluorination, intercalation, corrosion, and oxidation.

Molten salt can infiltrate the porous structure of graphite, leading to several detrimental effects. Entrapment of fissile products within the graphite pores can cause radiation damage and could pose challenges in the handling and disposal of contaminated components. The differential thermal expansion between the infiltrated salt and graphite, along with internal stress from pressurized molten salt and volumetric heating, can compromise the structural integrity of graphite. To mitigate these effects, employing ultra-fine graphite grades and applying sealants and coatings are effective strategies. A computational model based on coupled solid mechanics and heat transfer phenomena could be used to predict the internal stresses using Grizzly software.

In pebble-bed MSRs, graphite fuel pebbles can cause abrasion against reactor components due to friction and wear. The severity of wear is influenced by various factors such as temperature, environment, and the presence of lubricants. Tribological studies reveal that higher temperatures and molten salt environments, such as FLiBe, significantly reduce wear rates compared to dry conditions. Additionally, the chemical composition of the salt can further optimize graphite's tribological performance. Long-term wear effects can be modeled by incorporating surface defects into the geometry and predict stresses under thermal and radiation effects using Grizzly software.

Chemical degradation of graphite in a molten salt environment can occur through fluorination and intercalation. Fluorination can occur via replacement of hydrogen or oxygen atoms, or at the active sites, but does not cause structural degradation. Intercalation, on the other hand, can lead to exfoliation, where layers of graphite separate and peel away, damaging the graphite. Protective coatings can enhance graphite's resistance to intercalation.

Graphite generally exhibits good chemical stability in molten salt environments, though it can corrode under specific conditions, particularly in the presence of impurities or oxidants. Studies have shown that protective coatings, such as plasma-sprayed partially stabilized zirconia (PSZ), can effectively prevent such degradation. Corrosion behavior varies significantly with different graphite grades and coating applications, underscoring the need for detailed studies on uncoated and coated graphite to understand and mitigate corrosion mechanisms in MSRs. Research indicates that the presence of oxidants and impurities can accelerate graphite degradation in molten salts, making it essential to explore acceptable impurity limits.

Oxidation is another critical degradation mechanism, leading to weight loss and structural damage due to the formation of CO and CO_2 from the reaction of carbon atoms with oxygen. This process creates new porosity and compromises graphite's integrity. While extensive research on graphite oxidation has been conducted for gas-cooled reactors, studies specific to MSRs are limited. Findings from the coal industry

suggest that molten alkali metal salts can significantly accelerate graphite oxidation, a hypothesis worth exploring for fluoride salts in MSRs. Understanding oxidation behavior in MSRs is vital for developing protective measures.

The analysis of post-irradiated graphite from the MSRE experiment demonstrated exceptional chemical compatibility with molten fluoride salt, suggesting that the extent of chemical attack on graphite largely depends on the salt's infiltration capability. Therefore, the use of ultra-fine grade graphite could help mitigate chemical degradation effects. Existing oxidation modeling capabilities in Grizzly, which use reaction-diffusion equations to model graphite-air interactions, could be adapted to simulate the chemical degradation effects of graphite in molten salt environments.

ACKNOWLEDGMENTS

The author thanks the following persons for their active participation in discussions, thoughtful questions, and valuable feedback—all of which significantly contributed to this report: U.S. Nuclear Regulatory Commission (NRC) staff, Drs. Joseph Bass, Raj Iyengar, as well as Matthew Gordon, and Alexander Chereskin, along with Idaho National Laboratory (INL) colleagues Drs. William Windes and Benjamin Spencer.

This manuscript was authored by Battelle Energy Alliance, LLC under contract no. DE-AC07-05ID14517 with DOE. The U.S. Government retains a nonexclusive, paid-up, irrevocable, worldwide license to publish or reproduce the published form of this manuscript, or allow others to do so, for U.S. Government purposes.

CONTENTS

1 INTRODUCTION

Molten-salt reactors (MSRs) are a type of Generation IV nuclear reactor that utilizes liquid salt as a coolant. The liquid salt is typically composed of fluoride or chloride salts, and the nuclear fuel can be either dissolved in the salt or used in the form of solid particles such as pebbles. Table 1 presents some of the MSR systems currently being developed, highlighting the type of salt used, the moderator material utilized, and other relevant information.

MSRs offer several advantages over light-water reactors (LWRs). For instance, they can operate at higher temperatures, approximately 700°C, resulting in improved electricity generation efficiency and greater process heat opportunities. Moreover, MSRs operate at near-atmospheric pressures compared to LWRs. This eliminates the need for large, expensive reactor pressure vessels and secondary containment structures, and could minimize the risk of major coolant leaks during accidents, thus improving overall reactor safety. Liquid-fuel-based MSRs do not require fuel assembly production reducing the need for fuel fabrication. Another advantage of MSRs is their ability to refuel online, meaning fuel can be added to the reactor while it is still running at full power. LWRs, on the other hand, require shutdowns to move or introduce new fuel. Online refueling capabilities improve the capacity factor* and economics of MSRs.

Table 1: Selected MSR systems under development along with fuel and moderator information

No.	Company	Country	Type	Fuel	Salt	Moderator	Potential application(s)	Ref.
1	Thorcon	USA	Liquid reactor	Uranium	NaF-BeF2-UF4	Graphite	Energy	[1, 2]
2	Flibe Energy	USA	LFTR	Uranium	LiF-BeF2-UF4	Graphite	Energy, shipping,nuclear medicine	[3]
3	Terrestrial Energy	Canada	IMSR	Uranium	Molten Fluoride + Uranium	Graphite	Energy, ammonia, green Hydrogen	[4]
4	Kairos Power	USA	KP-FHR	TRISO fuel pebbles	FLiBe	Graphite (ET-10)	Energy	[5]
5	Terra Power	USA	Fast reactor	Uranium	NaCl-MgCl2	-	Energy	[6, 7]
6	Moltex	Canada,UK	SSR-U	Uranium/Sodium	Fluoride eutectic salts	Graphite (Not in contact with the fuel)	Energy	[8, 9]
7	Moltex	Canada,UK	SSR-W	Higher actinides from conventional oxide fuel	Chloride fuel salt	-	-	[8]
8	Copenhagen atomics	Denmark	SMR	Thorium	F7LiThPu	Unpressurized heavy water	Energy	[10]
9	Exodys Energy (Elysium)	USA	MCSFR	DU, LEU, SNF, RGPu, WGPu, Th, Unat †	Chloride fuel salt	-	Energy	[11, 12]
10	Abilene Christian University (ACU)	USA	MSR	Uranium	LiF-BeF2-UF4	Graphite (ultrafine grade)	Research reactor	[13]

*The ratio of the net electricity generated (over the time considered) to the energy that could have been generated at continuous full-power operation during the same period.

†RGPu (Reactor-Grade Plutonium), WGPu (Weapons-Grade Plutonium), and Unat (Natural Uranium).

MSRs offer many other advantages in addition to the ones mentioned above; however, they also carry certain limitations. One of their most notable drawbacks is the potential for radioactive fission products to deposit on components throughout the primary coolant system, potentially resulting in issues such as material degradation stemming from direct contact with the molten fuel salt. In MSRs that use lithium-based salts, tritium could be produced, which is both radioactive and mobile. Furthermore, remote maintenance becomes necessary due to components that are contaminated with highly radioactive fission products in the reactor, leading to higher operating costs.

This report specifically focuses on the degradation aspects of nuclear graphite material in a molten salt environment. Nuclear graphite is commonly used as a moderator and a reflector in MSR systems. In this report, we present details on various potential degradation mechanisms—information gathered from the literature and via consultations with subject matter experts. Figure 1 concisely summarizes the potential degradation mechanisms, incorporating details from reference [5] along with additional information. There are two main categories of degradation mechanisms: physical and chemical. Infiltration and abrasion/erosion are categorized as physical degradation mechanisms. The chemical category includes processes such as fluorination, intercalation, corrosion, and oxidation. A detailed review of each of the above mechanisms is provided in later sections of this report. Furthermore, the existing modeling approaches for a few critical graphite degradation mechanisms are briefly described, and potential modeling approaches are proposed where none exists.

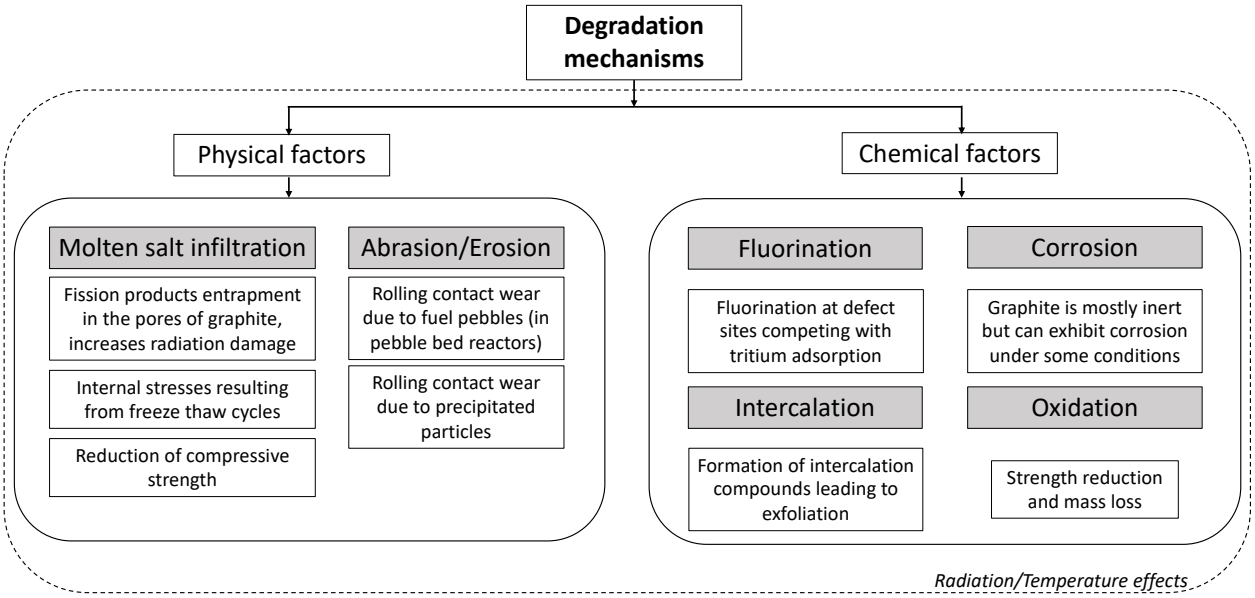

Figure 1: Summary of potential degradation mechanisms for graphite in a molten salt environment.

2 DEGRADATION MECHANISMS

This section explores the mechanisms that can lead to the degradation of nuclear graphite in molten salt environments. These mechanisms are categorized as either physical or chemical in nature.

2.1 Physical Factors

Within the realm of physical degradation, two significant mechanisms are observed: infiltration and erosion/abrasion. This subsection delves into the specifics of each mechanism, outlining their nature, potential impact on graphite, and modeling methodologies.

2.1.1 Infiltration

Molten salt directly contacts the moderator material in most MSR designs. Nuclear graphite, which is commonly used as a moderator, has a porous microstructure due to its manufacturing process. Graphite pores that are interconnected in a network that opens to the surface are known as open porosity, while others that are not connected to the surface are referred to as closed porosity. Some common nuclear graphite grades, along with the related microstructure and porosity information, are provided in Table 2.

Table 2: Different graphite grades, along with microstructure and porosity information [14]

No.	Grade	Type[a]	Grain size[b] (μm)	Bulk density[c] ($g.cm^{-3}$)	Open pores volume[d] ($cm^3.g^{-1}$)	Porosity[e] (%)	Pore dia[f] (μm)
1	POCO ZXF-5Q	microfine	1	1.8	0.083	20	0.5
2	POCO AXF-5Q	ultrafine	5	1.73	0.102	23	0.9
3	POCO TM	superfine	10	1.73	0.102	23	2
4	IG-110	superfine	10	1.76	0.079	21	3.9
5	2114	superfine	13	1.81	0.071	19	3.5
6	ETU-10	superfine	15	1.74	0.098	22	3.6
7	NBG-25	fine	60	1.81	0.068	19	5.1
8	CGB	medium-fine	–	1.86	0.003	17	0.2
9	PGX	medium-fine	460	1.76	0.055	22	5.6,30
10	NBG-17	medium-fine	800	1.85	0.042	17	3,12,51‡
11	PCEA	medium-fine	800	1.77	0.065	21	64
12	NBG-18	medium-coarse	1600	1.86	0.044	17	12

[a] *As per ASTM D8075-16;* [b] *No information was found on CGB;* [c] *ORNL data from physical measurements according to ASTM C559-163;* [d] *Calculated as per the volume-mass-density relation:* $V_0 = m(\frac{1}{\rho_{bulk}} - \frac{1}{\rho_{skeleton}})$; [e] *Calculated as per the equation* $V_{total} * \rho_{bulk} * 100\%$; [f] *Calculated using mercury porosimetry*.

Utilizing data compiled from various sources (as presented in reference [15]), it is inferred that most molten salts display a non-wetting behavior when in contact with graphite, characterized by a contact angle that exceeds 90°. Consequently, such non-wetting liquids do not spontaneously infiltrate the graphite pores but require a minimum pressure differential (ΔP) for infiltration, as described by the Young-Laplace equation:

$$\Delta P = -\frac{4\gamma \cos\theta}{d} \tag{1}$$

‡It should be noted that the characteristic pore diameters of NBG-17 exhibit a tri-modal distribution.

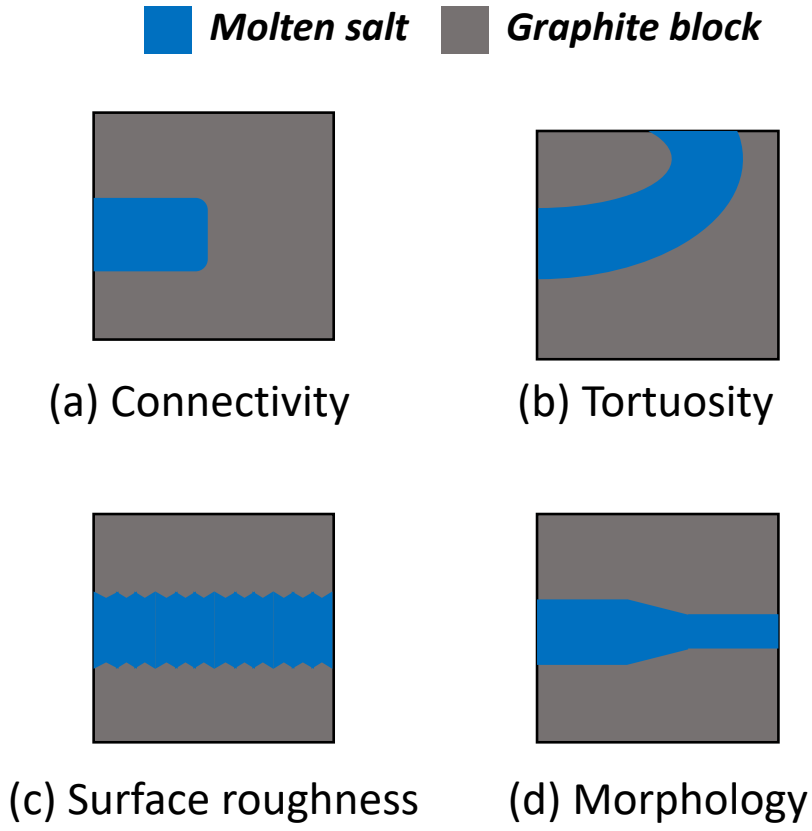

Figure 2: Schematic of microstructural features affecting the flow of molten salt.

It is essential to note that the magnitude of ΔP depends on the surface tension (γ)[§], contact angle (θ), and diameter of the pore (d). Equation 1 predicts whether a given salt will infiltrate the open pores in graphite. However, once the salt infiltrates the pores, its flow characteristics (e.g., velocity and stoppage) also depend on the features of the graphite's internal microstructure. Figure 2 provides a 2D schematic of important features of the graphite's internal microstructure that can influence the flow characteristics. It should be noted that these are simplified representations of the graphite microstructures and only intended to aid in this discussion of salt flow mechanisms[¶]. In Figure 2, the gray colored region represents the solid skeleton of the graphite material, and the blue colored region represents a porous channel within the graphite material that is completely filled with the molten salt. Four different features are identified that can influence the flow characteristics. They are as follows:

- Connectivity: In a microstructure, a porous channel may not extend entirely through the material, potentially terminating within the microstructure itself. In this scenario, flow stops once an open channel ends inside the microstructure.
- Tortuosity: Due to gravity and curvature effects, tortuosity affects the flow.
- Surface roughness: Due to friction, surface roughness reduces the flow velocity.

[§]Surface tension is highly dependent on the composition and purity of the material [16, 17]. Therefore, chemistry control is a crucial factor to consider in conjunction with salt infiltration.

[¶]Interested readers can refer to reference [18] for an understanding of the actual 3D graphite microstructures obtained through X-ray computed tomography.

- Morphology: Changes in pore morphology affect the flow. For example, as shown in Figure 2(d), if the pore constricts, the flow may decrease in velocity or otherwise stop altogether, as higher pressures are required to drive the flow, as per Equation 1.

Infiltration curves can be either obtained via mercury porosimetry or through direct salt intrusion studies [15]. Figure 3 gives a plot of mercury intrusion in various graphite grades, displaying the cumulative intrusion volume of mercury as a function of mercury pressure. Notably, higher pressures are required to infiltrate the smaller pores, as implied by Equation 1, which indicates an inverse relationship between the pressure differential and the pore diameter. Moreover, this relationship is evident in Figure 3. For example, when comparing the plots of PCEA and ZXF-5Q, it becomes apparent that PCEA, with a median pore diameter of 64 µm, initiates infiltration at approximately 1 psia, whereas ZXF-5Q, having a pore diameter of 0.5 µm, begins infiltration at around 300 psia. Also, note that at very high pressures, the internal microstructure can be damaged as indicated inside the red box as depicted in Figure 3. However, such high pressures (greater than 10000 psia) are unlikely in the normal operation of MSRs.

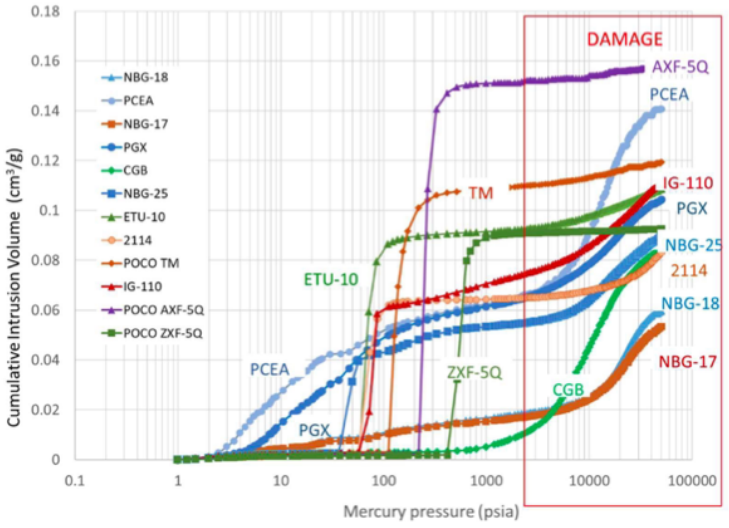

Grade	Avg. pore dia (µm)
NBG-18	12
PCEA	64
NBG-17	3,12,51
CGB	5.6,30
NBG-25	5.1
ETU-10	3.6
2114	3.5
TM	2
IG-110	3.9
AXF-5Q	0.9
ZXF-5Q	0.5

Figure 3: Mercury intrusion studies and the average pore diameters of various graphite grades [14].

Based on Equation 1, we can predict molten salt infiltration curves based on the results from mercury intrusion experiments, with the following equation [15]:

$$\Delta P_{salt} = \Delta P_{Hg} \frac{\gamma_{salt} \cos\theta_{salt}}{\gamma_{Hg} \cos\theta_{Hg}} \tag{2}$$

where ΔP_{Hg}, γ_{Hg}, and $\cos\theta_{Hg}$ represent the pressure differential, surface tension, and wetting angle of mercury on graphite, respectively. Similarly, ΔP_{salt}, γ_{salt}, and $\cos\theta_{salt}$ depict the same quantities for salt with salt infiltration.

Mercury intrusion porosimetry is supported by international standards and can be rapidly performed in specialized laboratories. Thus, this technique is highly convenient for those engaged in developing, testing, and manufacturing new graphite grades for MSRs, especially during the selection and production phases. However, note that the reliability of the correlation between the mercury intrusion data and the molten salt infiltration behavior depends on the accuracy of the molten salt data with regard to surface tension and contact angle [14]. Caution should be exercised in interpreting these correlations, as they have not yet been fully validated.

Multiple research groups have conducted direct salt infiltration studies[‖], employing various graphite grades and quantifying the weight change and volume of infiltrated salt [14, 19–25]. Figure 4 shows a compilation of plots of cumulative salt-infiltrated volume against the absolute salt pressure for select graphite grades. Both FLiNaK and FLiBe salts were used to generate the data in the figure. In the Molten-Salt Reactor Experiment (MSRE), 0.5 vol.%[**] salt infiltration into graphite was the design goal, and 4 vol.% and above was deemed unacceptable for reactor control [26]. If we compare the 4 vol.% criteria to experimental infiltration results shown in Figure 4, it is evident that of the select grades only ZXF-5Q, UGG-2, NG-CT-50, and G2 would have experienced acceptable levels of infiltration [15].

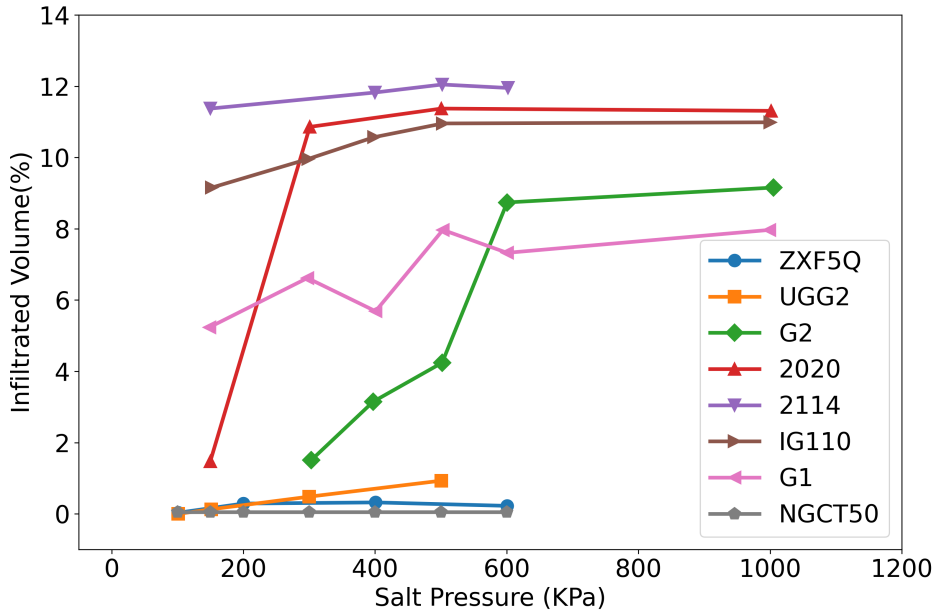

Figure 4: Infiltrated salt volume as a function of absolute salt pressure for select graphite grades, replotted from the figure provided in reference [15].

Molten salt infiltration into graphite pores can result in the following degradation effects:

(i) **Entrapment of fission products**

Molten salt can carry fissionable materials and fission products into the graphite pores. Fission and radioactive decay of those materials can inflict radiation damage on the graphite. Additionally, these processes can act as local heat sources and alter the heat transfer and mechanical deformation of graphite. Furthermore, the entrapped fission products can pose significant challenges in the handling and disposal of contaminated components.

(ii) **Internal stress**

Internal stresses in MSR graphite components can stem from several factors, including the coefficient of thermal expansion (CTE) mismatch between salt and graphite, pressurized molten salt in the pores, volumetric heating (see point [i]), and crystalline pressure. H. Zhoutang et al. conducted experiments

[‖]Salt intrusion studies are conducted using ASTM std. 8091-16.

[**]Volume percent is with respect to the total volume of the graphite specimen [14].

to measure the bulk thermal expansion of both pristine graphite and graphite infiltrated with salt across a range of different temperatures [27]. The resulting thermal expansion behavior is illustrated in Figure 5. Similar studies were also reported in references [25, 28]. Close examination of Figure 5 reveals that the thermal expansion of pristine graphite follows a linear trend. However, in the case of graphite infiltrated with salt, a distinct bilinear behavior is observed, as characterized by a noticeable kink that occurs precisely at the melting point of the FLiNaK salt (i.e., 450°C). This behavior arises from the significant difference in CTE between solidified salt (3.8e-5 K^{-1}) and graphite (4.5e-6 K^{-1}), with salt expansion being an order of magnitude greater below its melting point [28]. Consequently, below this temperature, the thermal expansion curve for infiltrated graphite is steeper than for pristine graphite. Above the melting point, the curve's slope aligns with that of pristine graphite as a result of additional salt melting and leaking from the pores, bringing the CTE of infiltrated graphite closer to that of pristine graphite [28].

Thus, before reaching the melting point, the difference in CTE between graphite and molten salt can generate thermal stresses in the graphite material [25, 28]. Furthermore, W. Qi et al. discuss the crystallization pressure[††], with crystallization of FLiNaK in the graphite pore creating pressure against the pore wall as a result of thermal dynamics [28]. This pressure is corroborated by a decrease in the d(002) spacing of the graphite, as measured using x-ray diffraction [28].

During a freeze-thaw cycle that could occur in the circumstance that the reactor core is drained, cooled, and then reheated, the thermal stresses and crystalline pressure can potentially induce internal stresses.

In contrast to the above discussion, which suggests that thermal cycling can inflict damage on salt-infiltrated graphite, studies conducted during the MSRE era indicate that thermal cycles do not impact the integrity of infiltrated graphite. According to reference [26], samples of CGB graphite, a fine-grade graphite with sub-micron pore size, were infiltrated with MSRE fuel salt at a gauge pressure of 1 kPa, and subjected to 100 freeze-thaw cycles ranging from 200°C to 700°C. No damage was indicated when analyzing the quantity and size of graphite cracks following the cycling process [26]. This disparity is likely attributable to the microstructure of the CGB graphite, which resulted in minimal salt infiltration under those specific conditions.

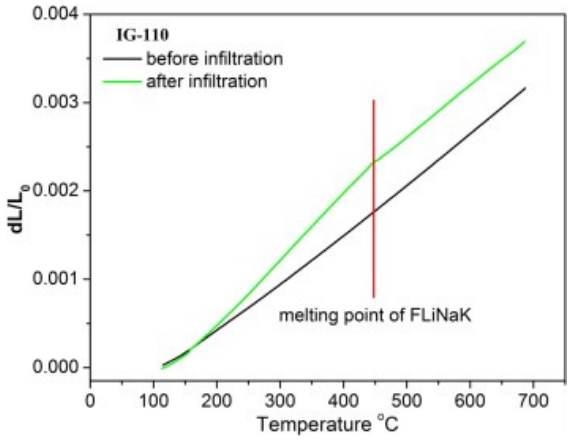

Figure 5: Comparison of the thermal expansion of graphite before and after molten salt infiltration [27] (*Reproduced with permission from Elsevier).*

[††]Crystallization pressure refers to the pressure exerted on the walls of a porous material due to the crystallization of an overcooled melt (such as salt) within its pores.

(iii) **Decrease of compressive strength**

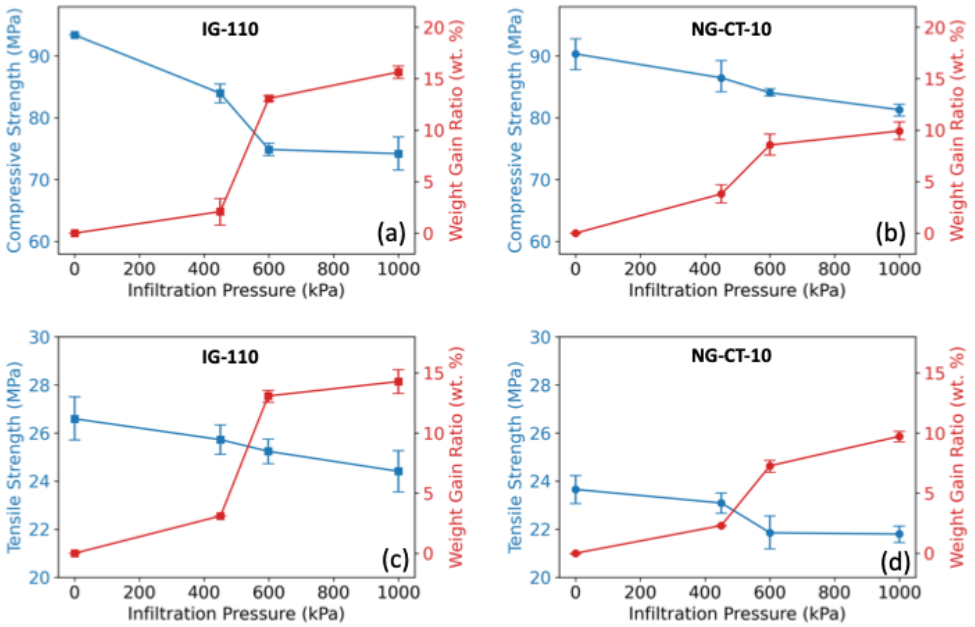

Figure 6: Influence of salt infiltration on the compressive strength of (a) IG-110 and (b) NG-CT-10 graphite grades, and tensile strength of (c) IG-110 and (d) NG-CT-10 graphite grades (*Replotted from reference [25]*).

C. Zhang et al. analyzed the effects of molten salt infiltration on tensile and compressive strength, and investigated the mechanism of failure under compressive loads [25]. Their study, which utilized FLiNaK as the salt, examined two graphite grades: IG-110 and NG-CT-10. The graphite samples were degassed before being immersed in the molten salt. The infiltration pressure, controlled by the pressure of the argon blanket gas, varied from 450 kPa to 1000 kPa. Once the salt was heated to 700°C and melted, the graphite samples were immersed and subjected to different pressures for 20 hours to allow for infiltration. Before the molten salt solidified, the graphite samples were removed to separate them from the salt. The pressure vessel was then cooled to room temperature while maintaining the gas overpressure. To minimize graphite oxidation during the experiment, high-purity argon (99.999%) was used.The weight change after infiltration was determined by weighing the graphite in a dry (H2O < 1 ppm), low oxygen (O2 < 1 ppm) argon atmosphere glove box.

Mechanical testing was conducted using a High-Temperature Universal Testing Machine (HTUTM). The samples, which had been infiltrated with molten salt, were removed from the glove box and transferred to the HTUTM in a hermetically sealed bag. To minimize graphite oxidation, high-purity argon (99.999%) was used throughout the experiment.Before testing, the high-temperature chamber was evacuated and then filled with argon. The samples were subsequently heated at a rate of approximately 10°C/min to 700°C and maintained at this temperature for about 60 minutes. Following this, the samples were subjected to uniaxial tension and compression. The results for compressive strength and tensile strength, as a function of infiltration pressure, are presented in Figures 6 (a) and (b), respectively.

From Figure 6, the following observations can be made: (a) the compressive strength of IG-110 decreased by approximately 20% and the compressive strength of NG-CT-10 decreased by approximately 10% in comparison to the non-infiltrated samples, and (b) the tensile strength was reduced by approximately 8% for both grades in comparison to the non-infiltrated sample. Furthermore, the

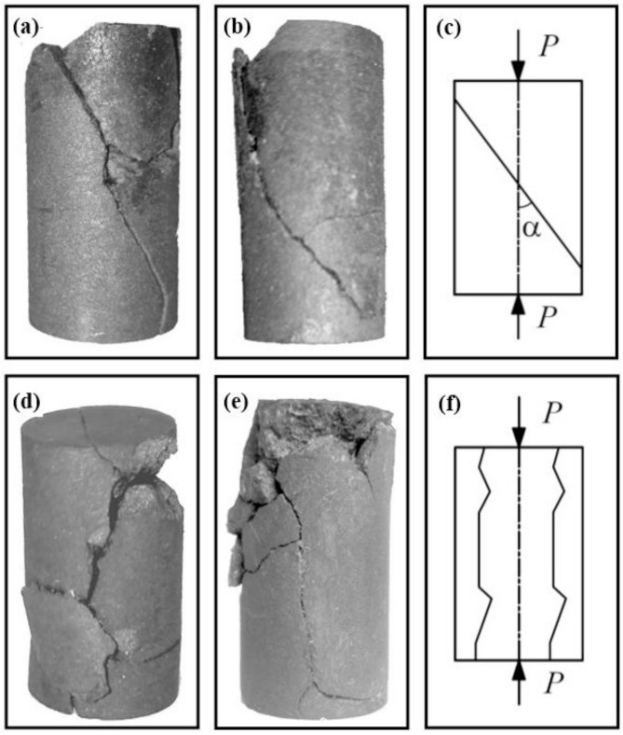

Figure 7: Images of reassembled major fragments and schematic representations of failure mechanisms observed during uniaxial compression testing: (a) virgin IG-110, (b) virgin NG-CT-10, (c) schematic of shear fracture, (d) molten infiltrated IG-110, (e) molten infiltrated NG-CT-10, and (f) schematic of longitudinal splitting fracture [25] (*Reproduced with permission from Elsevier*).

authors analyzed the fracture types of the above graphite grades during compression failure. Figure 7 shows images of reassembled major fragments and provides schematic representations of the failure mechanisms observed during uniaxial compression testing. It also illustrates the transition of the fracture mechanism from shear fracture in non-infiltrated graphite samples to longitudinal splitting fracture in infiltrated samples.

All the above-mentioned degradation aspects relate to the graphite's structural integrity, which is potentially compromised by pressurized molten salt in the pores of the graphite, volumetric heating of the molten salt (if fuel is also dissolved) in those pores, the difference in the coefficient of thermal expansion (CTE) between the salt and graphite, and the reduced strength of the graphite. A computational model based on coupled solid mechanics and heat transfer phenomena could be used to predict the internal stresses due to infiltration effects using Grizzly software [29]. Furthermore, the effects of irradiation could also be added to assess the graphite component's performance in an integrated manner using Grizzly software.

Based on the preceding discussion, it becomes evident that utilization of ultrafine graphite grades with micron-sized pores is a potential strategy for minimizing salt infiltration. Another avenue explored in the literature involves the application of sealings and coatings. This includes pyrolytic carbon (PyC), glassy carbon (GC), and silicon carbide (SiC) coatings, as well as composite approaches combining multiple barrier types. However, delamination of coating is a major concern due to the potential mismatch in thermally- or irradiation-induced dimensional changes between the coating and graphite. As an alternative to coatings, researchers are exploring pore-filling techniques (e.g., fixed-bed deposition and resin impregnation) to block open pores in graphite materials [30].

Multiple studies have shown the effectiveness of coatings and pore-filling techniques in preventing infiltration. In investigating the use of isotropic PyC as a barrier coating for IG-110, He et al. observed a significant reduction (23-fold) in FLiNaK infiltration as compared to uncoated graphite [31]. Similar findings were documented by Song et al. in their research on rough laminar PyC [32]. Bernadet et al. concluded that employing a dual coating layer comprised of a PyC interlayer and a GC top layer resulted in minimal infiltration [33]. Additionally, He et al. reported that graphite coated with SiC exhibited less than 1.1% weight gain in FLiNaK after 24 hours of exposure at 650°C [34]. Lastly, He et al. showed that phenolic resin impregnation completely prevented infiltration into IG-110 graphite [35].

2.1.2 Erosion and Abrasion

In pebble-bed molten salt reactors, resinated graphite fuel pebbles can rub against each other and the system's structural components due to coolant circulation and cycling of pebbles through the reactor. This occurs within both the molten salt environment and in areas where the pebbles lack salt coverage. The literature offers two comprehensive studies on the tribology of graphite-graphite and graphite-stainless steel (SS), as covered in the subsections below.

(i) **Tribology of Graphite-Graphite**

In their study, Vergari et al. conducted tribological experiments to investigate the friction and wear characteristics of different types of graphite, both in a dry argon environment and a wet FLiBe (molten salt) environment [36].

In the first set of studies, experiments were conducted in an argon environment at two different temperatures: room temperature (RT) and 600°C (HT). This study focuses on ET-10 nuclear graphite. Tribological measurements were carried out using a pin-on-disk tribometer, and various characterization techniques were employed to analyze wear spots. Before conducting the tests, the spheres (located at the tip of the pins) and the discs were degassed at 600°C to eliminate any adsorbed oxygen and moisture.

The results reveal a significant contrast between the RT and HT tests. The RT tests showed higher average coefficients of friction (COFs)—at 0.55—whereas the HT conditions resulted in a 1.5-fold reduction in COF, for an average of 0.33. Specific wear rates exhibited a similar trend, with RT wear rates being 0.4 ug/Nm, significantly higher than the 0.06 ug/Nm observed in the HT tests, marking a 6.7-fold reduction. Profilometry analysis identified the presence of a tribo-film (self-lubricating film) whose thickness was 10 microns for RT and 50 microns for HT wear spots, respectively.

The authors provide the following points to explain the discrepancy between RT and HT: At HT, the results indicate a more stable and mechanically resilient tribo-film, characterized by increased thickness and continuity. This enhanced film at HT provides improved lubrication, reducing the COF and wear in contrast to RT. The existence of temperature hysteresis further supports the argument, showing that the film maintains its effectiveness at intermediate temperatures before finally degrading at RT.

In the second set of experiments, ET-10 and IG-11 graphite grades were tested in a FLiBe environment. These experiments employed a ball-on-three-plates configuration within an argon glovebox, with a rotating shaft coming into contact with the three graphite plates. Prior to testing, all samples underwent a degassing process for 4 hours at 600°C to remove absorbed moisture and oxygen. Tests were performed at four different temperatures, ranging from 500°C to 600°C. The COFs and normalized wear rates (NWRs) were determined. Benchmark tests were also conducted in argon (dry sliding).

Results at 600°C indicated that the average COF values were approximately 1.3–1.55 times lower in a FLiBe environment than in an argon one, and the NWR was about 1.5–2 times lower in FLiBe than in argon. The temperature-dependent tests suggested the COF to be independent of temperature, whereas the NWR increased with temperature. The impact of salt chemistry was assessed by adding 1 wt% CrF_2, 1 wt% AgF, and 1 wt% Be. The results showed significant changes in both NWR and COF. The test involving CrF_2 resulted in dry sliding due to the lack of salt on the contact points, and this test is not discussed in this report. However, a lower COF and NWR were observed for the other two compositions, with Be having the lowest values. In comparison to FLiBe, the addition of Be resulted in average COFs and NWRs that were 4 and 2 times lower, respectively.

By applying the Hamrock and Dowson equation [37], the authors calculated the thickness of the FLiBe film at the contact interface and compared it to the composite roughness. This analysis revealed that sliding in FLiBe occurs in a boundary lubrication regime. Boundary lubrication is known to reduce adhesion forces between surfaces but is typically too thin to prevent mechanical abrasion caused by surface asperities. This suggests that FLiBe is particularly effective at reducing friction and wear, potentially more so than the formation of a graphite film.

The observed behavior in tests at different temperatures supports the hypothesis that FLiBe physically interposes itself between mating surfaces, thereby reducing adhesion. Additionally, there is evidence of chemical interactions between FLiBe and graphite, resulting in the formation of covalent C-F bonds at crystallite edges. This chemical reaction hypothesis is supported by the COF behavior during consecutive runs at different temperatures, showing hysteresis and irreversible changes in COF values. Furthermore, the research suggests that salt chemical reactivity can be influenced by the addition of metal fluorides, which impacts the salt's redox potential and subsequently its lubricating properties. The study also identifies a different lubrication mechanism—potentially related to salt wetting or the precipitation of Be metal—that may be at play when Be is added to FLiBe. Further investigations, including contact angle measurements, energy dispersive spectroscopy (EDS), and x-ray photoelectron spectroscopy (XPS) analysis, are needed to explore these mechanisms in greater detail.

(ii) **Tribology of Graphite-Stainless Steel**

In reference [38], lab-scale experiments were performed to understand the tribocorrosion behavior of graphite sliding against FLiNaK-lubricated 316H SS in an argon environment. The tribological tests were performed using a pin-on-disk configuration—with a graphite pin and a 316H SS disk—on a high-temperature tribometer equipped with an environmental control chamber. Three factors—temperature, sliding velocity, and salt volume (i.e., amount of lubrication)—were of primary interest in regard to impacting tribological behavior. The below paragraphs detail the role of each parameter.

(i) **Role of temperature**

Studies were performed at two different temperatures (i.e., 550°C and 650°C), with the other two parameters (i.e., sliding velocity and salt volume) being held constant. Figure 8 displays the obtained measurements of the COF and the wear of the graphite pin and SS flat. The outcomes indicate that the levels of friction and wear are lower at 550°C. The COF ranges between 0.1 and 0.15 at 550°C, and varies from 0.1 to 0.25 at 650°C. At 550°C, the pin and flat wear volumes were 0.012 and 0.009 mm^3, respectively. At 650°C, the wear volume doubled and the flat volume seemingly tripled. The authors hypothesize that three factors are behind the additional friction and wear at 650°C:

- Insufficient lubrication at 650°C, attributed to a 40% decrease in viscosity.

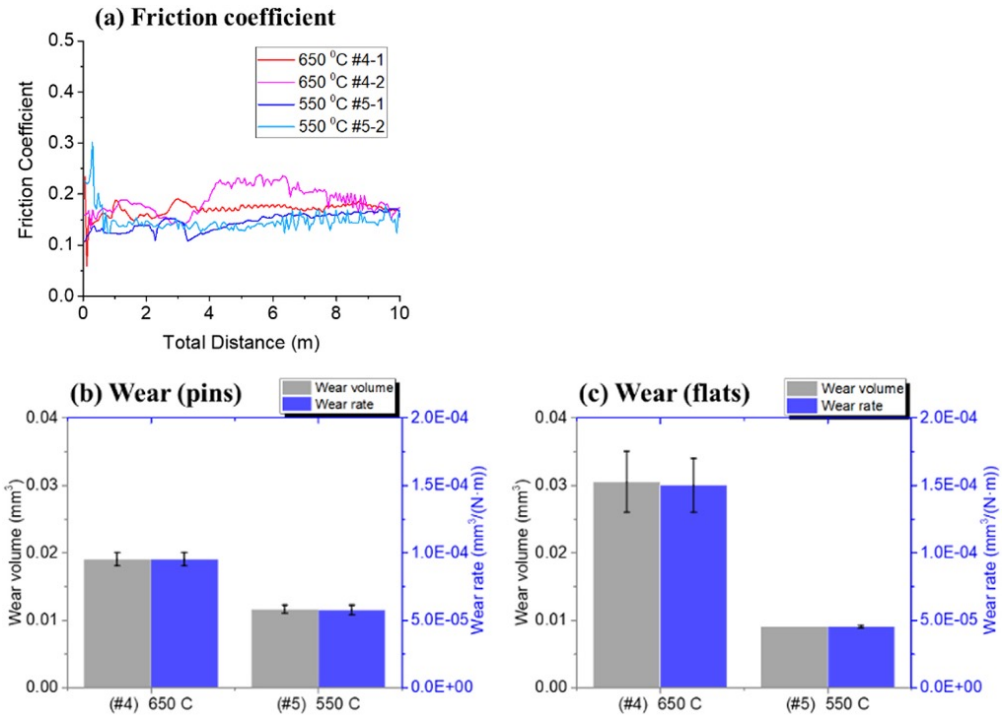

Figure 8: Role of temperature on the (a) COF, (b) wear of graphite pins, and (c) wear of SS flats [38] (*Reproduced with permission from Elsevier*).

- Enhanced corrosion of SS at 650°C in comparison to 550°C. In contrast, graphite is relatively chemically inert.
- Softening of SS at higher temperatures

(ii) **Role of sliding velocity**

Material testing was performed at three different sliding velocities (1, 10, and 100 mm/s), with the other two parameters being held constant. It is important to note that these tests were conducted over a total duration of 10000 seconds, resulting in varying sliding distances for each test case. The results for the COF and the wear of the graphite pin and SS flat are shown in Figure 9. COFs of 0.15, 0.15, and 0.1 were obtained for sliding velocities of 1, 10, and 100 mm/s, respectively. This is potentially due to the thicker lubrication at higher sliding velocities, per the Hamrock and Dowson formula [37]. The wear volume for both the graphite pin and SS flat is higher at 100 mm/s due to there being a larger sliding distance; however, the wear per unit distance is smaller. The graphite wear is higher than that of the SS flat wear at higher velocities, due to graphite's brittle behavior leading to more micro-fracture wear caused by vibration-induced impact.

(iii) **Role of salt volume**

To study the effect of salt volume on lubrication performance, three tests were carried out: (a) salt-less sliding (no salt, dry condition), (b) flooded lubrication (18 g of salt, fully submerged contact interface), and (c) starved lubrication (~6 g salt, partially submerged contact interface). The COF and wear characteristics from this study are given in Figure 10. The steady-state COF for all the salt quantities are within a range of 0.1–0.25. The dry condition led to material transfer from the graphite to the SS flats, whereas both lubricated cases experienced wear in the graphite pin as well as the SS flat. The starved lubrication resulted in more wear than the other cases,

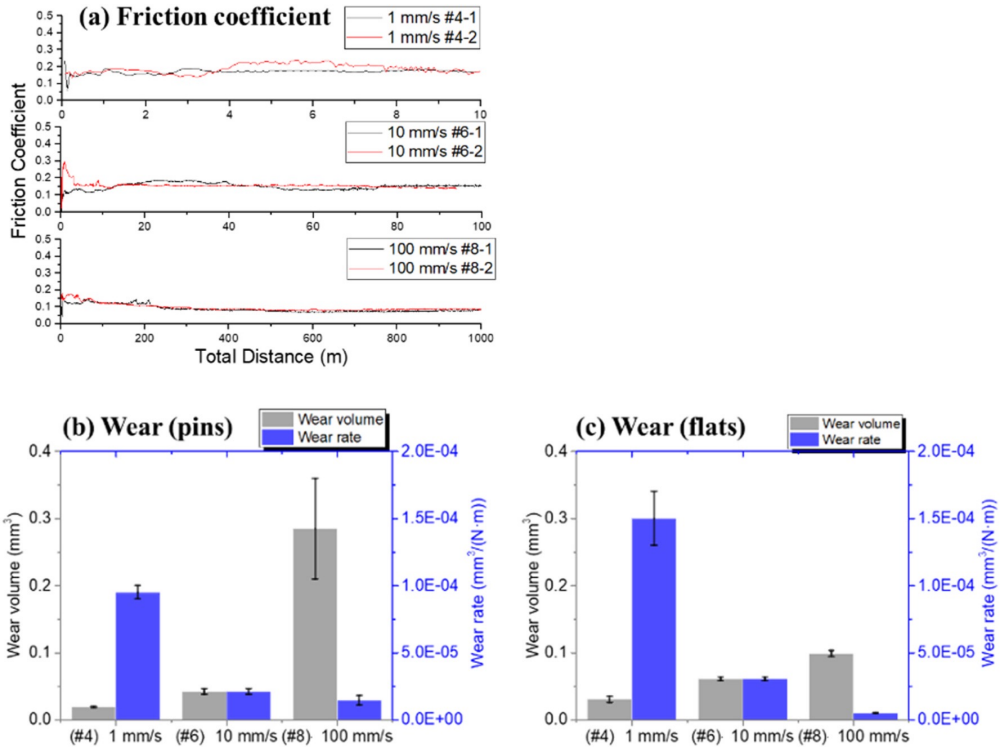

Figure 9: Role of sliding velocity on the (a) COF, (b) wear of graphite pins, and (c) wear of SS flats [38] (*Reproduced with permission from Elsevier*).

hypothetically due to the molten salt failing to provide effective lubrication and thus interfering with graphite deposition. As a result, a stable boundary lubrication or transfer deposit film could not be established, leading to poor wear performance.

For MSRs in which the nuclear fuel is dissolved in the salt, there is a possibility of erosion due to rolling contact wear that could occur as a result of precipitated particles carried by the molten salt from other areas of the reactor. However, it is important to note that no evidence of abrasion or erosion was found in the post-irradiation examination of graphite from the MSRE [39]. Therefore, more experimental evidence is needed to conclusively determine whether erosion/abrasion can be a limiting factor in MSRs containing fuel dissolved in the salt.

Phenomena such as abrasion and erosion cause wear to the graphite, leading to material loss and the formation of surface defects over the component's lifetime. These surface defects can be modeled using a diffuse interface approach and coupled with mechanical, thermal, and irradiation effects to understand the stress concentrations caused by wear. Grizzly software can be used for this integrated analysis, providing insights into the impact of these defects on the component's performance.

2.2 Chemical factors

In the domain of chemical degradation affecting nuclear graphite in molten salt environments, four major mechanisms play a key role: fluorination, intercalation, corrosion, and oxidation. This section explains each mechanism with their potential impact on the graphite material.

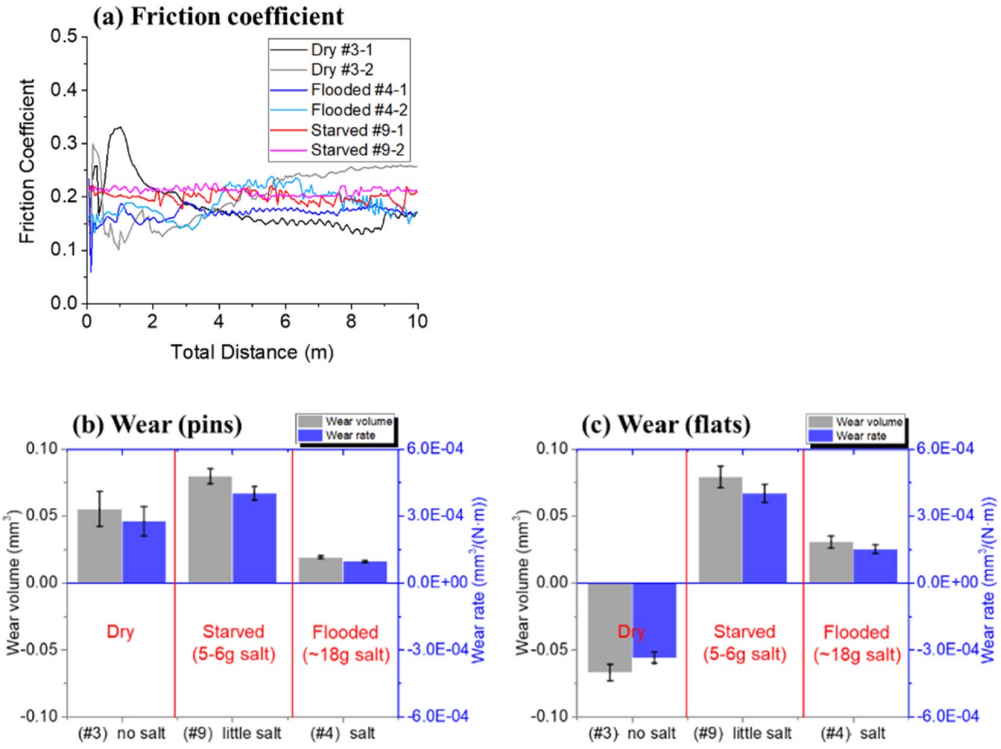

Figure 10: Role of salt volume on the (a) COF, (b) wear of graphite pins, and (c) wear of SS flats [38] (*Reproduced with permission from Elsevier*).

2.2.1 Fluorination

Fluorination of graphite in molten salt environments is a possibility. A few possible mechanisms for this, as provided in the literature, are as follows:

(i) **Fluorination through hydrocarbon and oxygen functional structure**

In nuclear graphite, C-H bonds are partly residual following graphitization of the raw materials. In a study by Yang et al. [40] on IG-110 grade nuclear graphite, CK-edge x-ray absorption near-edge structure revealed that the C-H bonds were uniformly distributed throughout the sample, and indicated that immersing the graphite in molten fluoride salts at 500°C for 16 hours resulted in the partial replacement of existing C-H bonds with C-F bonds. The chemical reactions of fluoride salts with graphite are generally thermodynamically unfavorable, so graphite is expected to be inert. To address this discrepancy, the authors of [41] hypothesized that it is uncertain whether degassing graphite at temperatures exceeding 800°C in order to remove chemisorbed hydrogen would result in fluorination. As gas composition measurements were not taken, it cannot be ruled out that the fluorination reported by Yang et al. [40] was caused by H_2O being present in their vacuum oven during the experiment. In the presence of LiF(g) and NaF(g) vapors, H_2O could have produced hydrogen fluoride (HF), which may have been responsible for the observed fluorination of the graphite. Furthermore, XPS results led the authors [41] to deduce that fluorination occurred as a result of replacing oxygen atoms in their study with graphite in FLiBe. The graphite sample initially had 11.1% relative peak area as oxygenated groups, which decreased to 0-7.9% after exposure to molten salt.

(ii) **Fluorination at active sites (edge sites)**

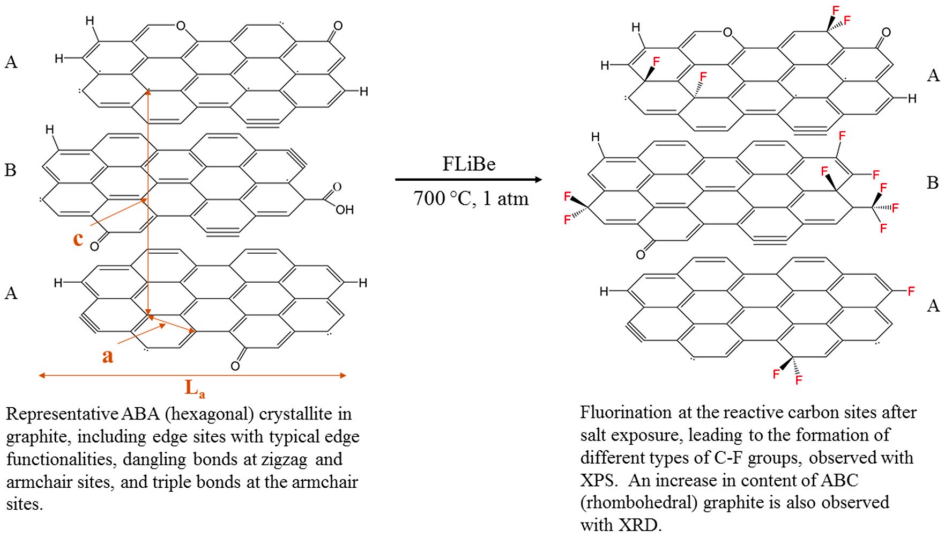

Figure 11: Possible reactive carbon sites leading to C-F bond formation upon FLiBe exposure [41] (*Reproduced with permission from Elsevier*).

Using XPS, Wu et al. observed fluorination of IG-110 graphite when immersed in molten FLiBe at 700°C for 12 hours [41]. They argued that certain carbon sites are more reactive than others, and that the fluorination may have occurred on those reactive sites[‡‡] (Figure 11). Analysis of the XRD and Raman data also revealed changes in the graphite's structure. These findings led them to propose that fluorination could introduce additional defects and active sites, potentially enhancing the chemisorption of tritium. This mechanism, however, is not known to cause any structural degradation of graphite.

(iii) **Intercalation**

Fluorination can also happen through intercalation, which is a mechanism discussed in detail in the following subsection.

2.2.2 Intercalation

Graphite intercalation compounds (GICs) can form when atoms or molecules (intercalants) are inserted between the layers of graphite, potentially leading to structural damage through exfoliation. Wu et al. suggested the possibility of fluorine GICs, based on their XPS analysis of molten FLiBe immersed in IG-110 graphite at 700°C for 12 hours [41]. Another study, this time led by Bernardet et al., involved experiments on nuclear graphite in powdered and disc forms, both in their raw state and with various coatings. These different graphite samples were impregnated with a Li-, Na-, and Zr-based fluoride molten salt at 500°C for 60 hours [33]. The results showed that, post-treatment, the c lattice parameter had increased from 6.758 to 6.771 Å for both the powdered and raw disc graphite, with a much smaller increase in the coated disc samples. However, in all cases, the increase in the lattice parameter was deemed too insignificant to confirm the formation of a fluorine-intercalated compound. Previous studies reported that the interlayer spacing for stage-1 fluorine-intercalated compounds typically falls within 9.38–9.44 Å; for stage-2, it is approximately 12.7 Å [43]. In their study, Sure et al. observed GIC formation when conducting experiments on uncoated

[‡‡]These are the same sites that are also susceptible to oxidation [42]. Potentially, fluorination and oxidation might be competing reactions. However, more studies need to be performed to fully understand this aspect.

high-density (HD) graphite in a molten LiCl–KCl eutectic salt at 600°C for up to 2000 hours. In contrast, when the graphite was coated with plasma-sprayed partially stabilized zirconia (PSZ), no intercalation compounds were observed [44]. Based on the available evidence, it is reasonable to conclude that coated graphite exhibits greater resistance to GIC formation than does uncoated graphite. The variation between the results found in references [33] and [44] may be attributable to the different graphite grades and exposure times. Furthermore, Takashima and Watanabe reported that, under specific conditions, graphite could react with a mixture of fluorine and hydrogen fluoride gases to form GICs [45].

2.2.3 Corrosion

The corrosion behavior of materials in the presence of molten salts at high temperatures has been extensively studied. Multiple research studies have revealed graphite to be chemically stable in molten salt environments, whereas a few other studies have shown that graphite can exhibit corrosion under certain conditions.

Multiple research articles have reported on the corrosion behavior of high-temperature structural alloys in the presence of molten fluoride salts at high temperatures. Some of these experiments were conducted using graphite crucibles; others employed crucibles made of materials such as nickel. Corrosion was noted to occur predominantly via the de-alloying of chromium (Cr) [46–50]. Weight loss due to corrosion was generally correlated with the initial Cr content of the alloys, and was consistent with the Cr content measured in the salts following the corrosion tests. Furthermore, the use of graphite crucibles accelerated the de-alloying of Cr and its deposition onto graphite, whereas this phenomenon was not very pronounced when other crucibles (e.g., Nickel) were used [47–49]. It must be highlighted that, while galvanic corrosion can affect the structural integrity of alloys near graphite, it does not significantly impact the structural integrity of the graphite material itself.

However, corrosion was observed in graphite, as reported in references [44, 51–53]. Sure et al. conducted a detailed study on the corrosion behavior of HD graphite and plasma-sprayed PSZ-coated HD graphite in a molten LiCl–KCl eutectic salt environment at 600°C over varying time periods [44]. Uncoated HD graphite exhibited weight loss due to corrosion. The molten salt corrosion mechanism in graphite involves three key processes: the formation of intercalation compounds, the adherence and diffusion of the salt into the graphite, and the filling of surface porosity with molten salt. This process begins when the molten salt penetrates through the pores of the graphite, interacts with the carbon atoms on the surface, and dislodges the atoms from its lattice. In contrast, PSZ-coated graphite showed weight gain due to salt deposits on the surface, but demonstrated excellent corrosion resistance, with no observable degradation on the coating's surface. This indicates the effectiveness of PSZ coatings in protecting graphite against a chemical attack by molten salt environments. Sure et al. pointed out that several oxidants and impurities in the molten salts also accelerate the degradation of HD graphite in LiCl–KCl salt by dissolution and leaching of the elements. This makes investigating the acceptable limits of impurities in graphite and molten salt a promising avenue for future research.

Additionally, Kamali et al. investigated microstructural changes in graphite by heating a mixture of synthetic polycrystalline graphite and lithium chloride to 1250°C [51]. Different forms of corrosion attack on the graphite occurred, leading to the formation of different microstructures comprised of exfoliated carbon sheets and nanosheets, pitted particles, and carbon nanorods. It is important to note that 1250°C is beyond the operating temperature range of MSRs. In another study, Vacik et al. investigated the interaction of molten FLiNaK with GC, pyrographite, and reactor-grade graphite at 540°C for up to 10 hours. Researchers found that reactor-grade graphite completely dissolved in FLiNaK after 10 hours, GC underwent a 0.5% weight

loss, and pyrographite remained completely stable [53]. However, the specific grade of reactor graphite used in the study is not specified, and no other research group has reported such an observation, leaving the exact cause of its complete dissolution unclear. Hence, further experimental research on molten fluoride salt corrosion of graphite is essential to elucidate the chemical stability of graphite against fluoride salts at various temperatures.

2.2.4 Oxidation

At elevated operating temperatures, graphite is susceptible to oxidation from impurities in the coolant or graphite itself. Oxygen has a high affinity for unsaturated carbon atoms present at the active edge sites, such as armchair or zig-zag configurations. It is at these locations that oxygen chemisorption occurs [54, 55].

The primary consequence of oxidation in regard to graphite is the weight loss that results from the formation of CO and CO_2 when carbon atoms react with oxygen. This gasification process leads to the formation of new porosity and networks of pores, making previously sealed porosity accessible. The extent of weight loss, changes in microstructure, and thickness of the region where oxidation occurs depend on graphite grade and temperature [56–58].

Extensive research has been conducted on graphite oxidation in gas-cooled [59, 60] and high-temperature gas-cooled [42, 56, 61] reactors. Nevertheless, studies on graphite oxidation in regard to MSRs have not gained widespread attention, causing uncertainty over whether molten salt environments would accelerate or decelerate the oxidation process.

The coal industry has, however, studied graphite oxidation in molten sodium carbonates and sulfates. This body of this research reveals that sodium alkali metal molten salts exhibit a catalytic effect on coal gasification, causing accelerated graphite oxidation when the graphite is immersed in a salt environment [62–65]. For example, at 900°C, graphite oxidation rates have been shown to surge by approximately 40-fold when the graphite is placed in a lithium carbonate salt environment [65]. While evidence for fluoride-salt-mediated oxidation remains insufficient, it represents an avenue worth exploring in future studies.

It is crucial to acknowledge that the analysis of post-irradiated graphite from the MSRE experiment demonstrated exceptional chemical compatibility between the molten fluoride salt and the graphite moderator [39]. The corrosion mechanism, as described by Sure et al. [44], suggests that the extent of chemical attack on graphite by molten salt largely depends on the salt's ability to infiltrate the graphite structure. Given that the MSRE used CGB grade graphite, known for its submicron characteristic pore diameter and consequently low infiltration rates, the observed compatibility is consistent with expected behavior. Therefore, using ultra-fine grade graphite could help mitigate chemical degradation effects. The existing oxidation modeling capabilities in Grizzly, which simulate graphite-air interactions using reaction-diffusion equations, could be modified to model chemical degradation effects.

3 SUMMARY

Degradation of nuclear graphite in molten salt environments is a critical consideration when designing and operating MSRs. This report has examined various degradation mechanisms, including both physical and chemical factors, to better understand the potential challenges associated with maintaining the structural integrity of graphite components in MSRs.

Among the physical factors, salt infiltration into graphite pores has been identified as one of the potential degradation mechanisms. The infiltration of molten salt into these open pores can lead to the entrapment of fission products, potentially causing radiation damage and raising safety concerns regarding the handling and disposal of contaminated graphite components. Moreover, the pressurization of pores from molten salt infiltration, the differential thermal expansion between the salt and graphite, and volumetric heating may induce internal stress, compromising the structural integrity of the graphite. Ideally, a nuclear graphite material that prevents infiltration would be preferred. Though complete prevention might pose as a challenge under different operating conditions, studies indicate that employing ultra-fine-grade graphite and applying sealants and coatings are effective strategies to minimize salt infiltration. A computational model capable of predicting salt infiltration based on graphite microstructure would significantly aid in rapidly assessing a material's susceptibility to infiltration. Additionally, experiments evaluating the durability of sealants and coatings under various temperatures and radiation levels would be beneficial. The current body of literature does not provide a definitive answer on whether the aforementioned factors will induce internal stress or to what extent. Therefore, a computational model to calculate internal stress based on coupled solid mechanics and heat transfer in Grizzly software is proposed to predict the internal stresses resulting from these factors.

Erosion and abrasion represent additional physical factors that can lead to the structural degradation of graphite components. This degradation often results from the interaction between solid particles, such as dust or fuel pebbles, and the surfaces of graphite components as they circulate within the system. Tribocorrosion experiments have detailed the impact of these interactions, revealing a complex relationship between material properties, environmental conditions, and lubrication. Notably, tribological studies on graphite have shown that wear and friction are most pronounced at lower temperatures under dry conditions. Conversely, higher temperature environments with FLiBe, a molten salt, significantly reduce friction and wear rates, highlighting the protective role of FLiBe against the more severe effects observed in dry sliding conditions. Furthermore, the chemistry of the salt was found to affect the tribological performance of graphite, with the addition of metal fluorides resulting in an enhanced performance. This suggests a promising avenue for optimizing the tribological behavior of graphite through careful manipulation of chemical additives in the lubricant. To further advance our understanding and capability in this area, a multi-faceted research approach would be beneficial. This includes comprehensive tribological testing across a broad spectrum of conditions—encompassing various temperatures, environments, and salt compositions. Through this comprehensive investigation, wear rates could be quantified under different conditions. Additionally, a computational model could be developed by modeling long-term wear effects as surface defects, and Grizzly software could be used to evaluate stresses due to combined thermal and irradiation effects.

Investigations into chemical degradation mechanisms affecting graphite, including fluorination, intercalation, corrosion, and oxidation, reveal varied impacts. While fluorination does not structurally degrade graphite, intercalation may cause damage through exfoliation. The application of protective coatings has shown promise in enhancing graphite's resistance to these processes. Corrosion and oxidation, both exacerbated by impurities, lead to significant weight loss and structural integrity loss. Studies on graphite oxidation in molten sodium carbonates and sulfates suggest that alkali molten salts accelerate graphite oxidation. However, there is no available research on fluoride-salt-mediated oxidation and it would be beneficial to conduct such experiments. Given these insights, it is beneficial to identify appropriate protective coatings

for graphite to enhance its resistance to the chemical attack mechanisms identified. Further research could be helpful to better understand the specific conditions under which each degradation mechanism is activated or accelerated, such as temperature thresholds, exposure times, and the presence of impurities. Furthermore, the post-irradiated graphite (CGB grade) analysis from the MSRE experiment revealed exceptional chemical compatibility with the molten fluoride salt. Given that CGB grade allows for limited infiltration, it would be reasonable to state that the extent of chemical attack on graphite by molten salt largely depends on the salt's ability to infiltrate the graphite. Therefore, the use of ultra-fine grade graphite could help mitigate chemical degradation effects. Existing oxidation modeling capabilities in Grizzly, which use reaction-diffusion equations to model graphite-air interactions, could be adapted to simulate the chemical degradation effects of graphite in molten salt environments.

REFERENCES

[1] D. Wilson, "ThorCon: Status 2022." https://msrworkshop.ornl.gov/wp-content/uploads/2022/11/38_Wilson_ThorCon-Status-2022-R1c-dfw.pdf.

[2] https://thorconpower.com/design.

[3] https://flibe.com/energy/.

[4] https://www.terrestrialenergy.com/technology/molten-salt-reactor/.

[5] "Graphite material qualification for the kairos power fluoride salt-cooled high-temperature reactor." https://www.nrc.gov/docs/ML2213/ML22132A205.pdf.

[6] B. M. Chisholm, "Development of TerraPower's Molten Chloride Fast Reactor (MCFR) to enable low-cost, economy-wide decarbonization." http://local.ans.org/savriv/wp-content/uploads/2021/06/SR-ANS-Brief_distributed.pdf, 2021.

[7] https://www.terrapower.com/our-work/molten-chloride-fast-reactor-technology/.

[8] I. Scott, "Stable salt reactors." https://msrworkshop.ornl.gov/wp-content/uploads/2020/11/24_Scott_Moltex_SSR_ORNL1.pdf, 2020.

[9] "Stable Salt Reactor – Uranium (SSR-U)." https://www.moltexflex.com/wp-content/uploads/SSR-U_Technical_Description-WEB-COPY_Final.pdf, 2022.

[10] https://www.copenhagenatomics.com/technology/.

[11] "Molten chloride salt fast reactor." https://thoriumenergyalliance.com/wp-content/uploads/2020/02/Elysium-MCSFR-TEAC10-Update.pdf.

[12] https://www.exodysenergy.com/.

[13] "Abilene christian university molten salt research reactor preliminary safety analysis report." https://www.nrc.gov/docs/ML2222/ML22227A203.pdf.

[14] N. C. Gallego, C. I. Contescu, and J. R. Keiser, "Progress report on graphite-salt intrusion studies," tech. rep., Oak Ridge National Laboratory, 2020.

[15] L. Vergari, M. Nelson, A. Droster, C. Contescu, N. Gallego, and R. O. Scarlat, "Infiltration of molten fluoride salts in graphite: Phenomenology and engineering considerations for reactor operations and waste disposal," *Journal of Nuclear Materials*, vol. 572, 12 2022.

[16] G. Mellors and S. Senderoff, "The density and surface tension of molten fluorides," in *Electrochemistry*, pp. 578–598, Pergamon, 1965.

[17] A. Nagashima, "Viscosity, thermal conductivity, and surface tension of high-temperature melts," *International Journal of Thermophysics*, vol. 11, no. 2, pp. 417–432, 1990.

[18] J. D. Arregui-Mena, D. Griffiths, R. N. Worth, C. E. Torrence, A. Selby, C. Contescu, N. Gallego, P. D. Edmondson, P. M. Mummery, and L. Margetts, "Microstructural characterization data of as received IG-110, 2114 and ETU-10 nuclear graphite grades and oxidation characterization data of IG-110," *Data in Brief*, vol. 44, p. 108535, 2022.

[19] Z. He, L. Gao, W. Qi, B. Zhang, X. Wang, J. Song, X. He, C. Zhang, H. Tang, H. Rohan, H. Xia, and X. Zhou, "Molten FLiNaK salt infiltration into degassed nuclear graphite under inert gas pressure," *Carbon*, vol. 84, pp. 511–518, 2015.

[20] P. Lian, J. Song, Z. Liu, J. Zhang, Y. Zhao, Y. Gao, Z. Tao, Z. He, L. Gao, H. Xia, Q. Guo, P. Huai, and X. Zhou, "Preparation of ultrafine-grain graphite by liquid dispersion technique for inhibiting the liquid fluoride salt infiltration," *Carbon*, vol. 102, pp. 208–215, 6 2016.

[21] Y. Zhong, J. Zhang, J. Lin, L. Xu, F. Zhang, H. Xu, Y. Chen, H. Jiang, Z. Li, Z. Zhu, and Q. Guo, "Mesocarbon microbead based graphite for spherical fuel element to inhibit the infiltration of liquid fluoride salt in molten salt reactor," *Journal of Nuclear Materials*, vol. 490, pp. 34–40, 7 2017.

[22] W. T. Zhang, B. L. Zhang, J. L. Song, W. Qi, X. J. He, Z. J. Liu, P. F. Lian, Z. T. He, L. N. Gao, H. H. Xia, X. D. Liu, X. T. Zhou, L. B. Sun, and X. X. Wu, "Microstructure and molten salt impregnation characteristics of a micro-fine grain graphite for use in molten salt reactors," *Xinxing Tan Cailiao/New Carbon Materials*, vol. 31, pp. 585–593, 12 2016.

[23] H. Tang, W. Qi, Z. He, H. Xia, Q. Huang, C. Zhang, X. Wang, J. Song, P. Huai, and X. Zhou, "Infiltration of graphite by molten 2LiF–BeF_2 salt," *Journal of Materials Science*, vol. 52, pp. 11346–11359, 10 2017.

[24] J. Song, Y. Zhao, J. Zhang, X. He, B. Zhang, P. Lian, Z. Liu, D. Zhang, Z. He, L. Gao, H. Xia, X. Zhou, P. Huai, Q. Guo, and L. Liu, "Preparation of binderless nanopore-isotropic graphite for inhibiting the liquid fluoride salt and Xe^{135} penetration for molten salt nuclear reactor," *Carbon*, vol. 79, pp. 36–45, 2014.

[25] C. Zhang, Z. He, Y. Gao, H. Tang, W. Qi, J. Song, and X. Zhou, "The effect of molten FLiNaK salt infiltration on the strength of graphite," *Journal of Nuclear Materials*, vol. 512, pp. 37–45, 12 2018.

[26] R. B. Briggs, W. H. Cook, and A. Taboada, "Modifications to Specifications for MSRE Graphite," tech. rep., Oak Ridge National Laboratory (ORNL), 1963.

[27] Z. He, L. Gao, X. Wang, B. Zhang, W. Qi, J. Song, X. He, C. Zhang, H. Tang, H. Xia, and X. Zhou, "Improvement of stacking order in graphite by molten fluoride salt infiltration," *Carbon*, vol. 72, pp. 304–311, 2014.

[28] W. Qi, Z. He, H. Tang, B. Zhang, C. Zhang, L. Gao, J. Song, D. Zhang, X. Wang, X. Du, G. Lei, H. Xia, J. Wang, P. Huai, and X. Zhou, "Effects of FLiNaK infiltration on thermal expansion behavior of graphite," *Journal of Materials Science*, vol. 52, pp. 4621–4634, 4 2017.

[29] B. W. Spencer, W. M. Hoffman, S. Biswas, W. Jiang, A. Giorla, and M. A. Backman, "Grizzly and BlackBear: Structural component aging simulation codes," *Nuclear Technology*, vol. 207, pp. 981–1003, Apr. 2021.

[30] J. J. Lee, J. D. Arregui-Mena, C. I. Contescu, T. D. Burchell, Y. Katoh, and S. K. Loyalka, "Protection of graphite from salt and gas permeation in molten salt reactors," 6 2020.

[31] X. He, J. Song, L. Xu, J. Tan, H. Xia, B. Zhang, Z. He, L. Gao, X. Zhou, M. Zhao, Z. Zhu, and S. Bai, "Protection of nuclear graphite toward liquid fluoride salt by isotropic pyrolytic carbon coating," 2013.

[32] J. Song, Y. Zhao, X. He, B. Zhang, L. Xu, Z. He, D. Zhang, L. Gao, H. Xia, X. Zhou, P. Huai, and S. Bai, "Preparation of pyrolytic carbon coating on graphite for inhibiting liquid fluoride salt and Xe^{135} penetration for molten salt breeder reactor," *Journal of Nuclear Materials*, vol. 456, pp. 33–40, 2015.

[33] V. Bernardet, S. Gomes, S. Delpeux, M. Dubois, K. Guérin, D. Avignant, G. Renaudin, and L. Duclaux, "Protection of nuclear graphite toward fluoride molten salt by glassy carbon deposit," *Journal of Nuclear Materials*, vol. 384, pp. 292–302, 2 2009.

[34] X. He, J. Song, J. Tan, B. Zhang, H. Xia, Z. He, X. Zhou, M. Zhao, X. Liu, L. Xu, and S. Bai, "SiC coating: An alternative for the protection of nuclear graphite from liquid fluoride salt," 2014.

[35] Z. He, P. Lian, Y. Song, Z. Liu, J. Song, J. Zhang, J. Feng, X. Yan, and Q. Guo, "Improving molten fluoride salt and Xe^{135} barrier property of nuclear graphite by phenolic resin impregnation process," *Journal of Nuclear Materials*, vol. 499, pp. 79–87, 2 2018.

[36] L. Vergari, *Chemistry and Physics of Graphite in Fluoride Salt Reactors*. PhD thesis, University of California, Berkeley, 2023.

[37] B. J. Hamrock, D. Dowson, and T. E. Tallian, "Ball Bearing Lubrication (The Elastohydrodynamics of Elliptical Contacts)," *Journal of Lubrication Technology*, vol. 104, pp. 279–281, 04 1982.

[38] X. He, C. Kumara, D. Sulejmanovic, J. R. Keiser, N. Gallego, and J. Qu, "Tribocorrosion of stainless steel sliding against graphite in FLiNaK molten salt," *Wear*, p. 204706, 6 2023.

[39] H. E. Mccoy and B. Mcnabb, "Postirradiation examination of materials from the MSRE," Tech. Rep. ORNL-TM-4174, Oak Ridge National Laboratory, 1972.

[40] X. Yang, S. Feng, X. Zhou, H. Xu, and T. K. Sham, "Interaction between nuclear graphite and molten fluoride salts: A synchrotron radiation study of the substitution of graphitic hydrogen by fluoride ion," *Journal of Physical Chemistry A*, vol. 116, pp. 985–989, 1 2012.

[41] H. Wu, F. Carotti, R. Gakhar, N. Patel, and R. O. Scarlat, "Fluorination of nuclear graphite IG-110 in molten 2LiF-BeF_2 (FLiBe) salt at 700ºC," *Journal of Fluorine Chemistry*, vol. 211, pp. 159–170, 7 2018.

[42] J. J. Kane, C. I. Contescu, R. E. Smith, G. Strydom, and W. E. Windes, "Understanding the reaction of nuclear graphite with molecular oxygen: Kinetics, transport, and structural evolution," 9 2017.

[43] T. Nakajima, M. Kawaguchi, and N. Watanabe, "Graphite intercalation compound of fluorine with lithium fluoride," *Synthetic Metals*, vol. 7, pp. 117–124, 12 1983.

[44] J. Sure, A. R. Shankar, S. Ramya, and U. K. Mudali, "Molten salt corrosion of high density graphite and partially stabilized zirconia coated high density graphite in molten LiCl-KCl salt," *Ceramics International*, vol. 38, pp. 2803–2812, 5 2012.

[45] M. Takashima and N. Watanabe, "Effect of hydrogen fluoride on the formation of graphite fluoride," *Nippon Kagaku Kaishi*, vol. 1976, no. 8, pp. 1222–1227, 1976.

[46] L. C. Olson, J. W. Ambrosek, K. Sridharan, M. H. Anderson, and T. R. Allen, "Materials corrosion in molten LiF–NaF–KF salt," *Journal of Fluorine Chemistry*, vol. 130, pp. 67–73, 1 2009.

[47] G. Zheng, B. Kelleher, L. He, G. Cao, M. Anderson, T. Allen, and K. Sridharan, "High-Temperature Corrosion of UNS N10003 in Molten Li_2BeF_4 (FLiBe) Salt," *Corrosion*, vol. 71, pp. 1257–1266, 10 2015.

[48] G. Zheng, B. Kelleher, G. Cao, M. Anderson, T. Allen, and K. Sridharan, "Corrosion of 316 stainless steel in high temperature molten Li_2BeF_4 (FLiBe) salt," *Journal of Nuclear Materials*, vol. 461, pp. 143–150, 6 2015.

[49] G. Zheng and K. Sridharan, "Corrosion of structural alloys in high-temperature molten fluoride salts for applications in molten salt reactors," *JOM*, vol. 70, pp. 1535–1541, 8 2018.

[50] R. Pillai, S. S. Raiman, and B. A. Pint, "First steps toward predicting corrosion behavior of structural materials in molten salts," *Journal of Nuclear Materials*, vol. 546, 4 2021.

[51] A. R. Kamali and D. J. Fray, "Molten salt corrosion of graphite as a possible way to make carbon nanostructures," *Carbon*, vol. 56, pp. 121–131, 5 2013.

[52] J. Sure and U. Kamachi Mudali, *Molten Salt Corrosion Behaviour of Graphite Materials*, pp. 143–168. Singapore: Springer Nature Singapore, 2022.

[53] J. Vacík, V. Hnatowicz, J. Ĉervená, R. Mach, and I. Peka, "Molten fluoride salts incorporation into pristine and ion-modified carbon allotropes and metallic foils," *Czechoslovak Journal of Physics*, vol. 49, pp. 997–1002, 1 1999.

[54] J. J. Kane, A. C. Matthews, W. D. Swank, and W. E. Windes, "Effects of air oxidation on the evolution of surface area within nuclear graphite and the contribution of macropores," *Carbon*, vol. 166, pp. 291–306, 9 2020.

[55] R. E. Smith, J. J. Kane, and W. E. Windes, "Determining the acute oxidation behavior of several nuclear graphite grades," *Journal of Nuclear Materials*, vol. 545, 3 2021.

[56] L. Xiaowei, R. Jean-Charles, and Y. Suyuan, "Effect of temperature on graphite oxidation behavior," *Nuclear Engineering and Design*, vol. 227, pp. 273–280, 2 2004.

[57] C. I. Contescu, T. Guldan, P. Wang, and T. D. Burchell, "The effect of microstructure on air oxidation resistance of nuclear graphite," *Carbon*, vol. 50, pp. 3354–3366, 8 2012.

[58] S.-H. Chi and G.-C. Kim, "Comparison of the oxidation rate and degree of graphitization of selected IG and NBG nuclear graphite grades," *Journal of Nuclear Materials*, vol. 381, pp. 9–14, 10 2008.

[59] B. J. Marsden, G. N. Hall, and A. N. Jones, "4.13 - graphite in gas-cooled reactors," in *Comprehensive Nuclear Materials (Second Edition)*, pp. 357–421, Oxford: Elsevier, second edition ed., 2020.

[60] J. Standring, "Calculation of the graphite weight-loss in civil magnox and advanced gas-cooled reactors," *Journal of Nuclear Energy. Parts A/B. Reactor Science and Technology*, vol. 20, no. 3, pp. 201–217, 1966.

[61] W. Windes, G. Strydom, R. Smith, and J. Kane, "Role of nuclear grade graphite in controlling oxidation in modular HTGRs," Tech. Rep. INL/EXT-14-31720, Idaho National Laboratory, 2014.

[62] G. B. Dunks, D. Stelman, and S. J. Yosim, "Graphite oxidation in sodium carbonate/sodium sulfate melts," *Inorganic Chemistry*, vol. 21, pp. 108–114, 1 1982.

[63] G. B. Dunks, D. Stelman, and J. Yosim, "Contribution from the rockwell international corporation graphite oxidation in sodium carbonate/sodium sulfate melts," 1982.

[64] D. Stelman, "Air oxidation of graphite in molten salts," *ECS Proceedings Volumes*, vol. 1976-6, pp. 299–314, 1 1976.

[65] D. McKee and D. Chatterji, "The catalytic behavior of alkali metal carbonates and oxides in graphite oxidation reactions," *Carbon*, vol. 13, pp. 381–390, 1975.